# Nano-Metal-Ink-Based Electrode Embedded in Parylene HARS with the Aid of the Capillary Effect

Takumi Tsutsumino[1], Yuji Suzuki[1], Noriko Sakurai[1], Nobuhide Kasagi[1], and Yoshihiko Sakane[2]

[1]Department of Mechanical Engineering, The University of Tokyo
Hongo 7-3-1, Bunkyo-ku, Tokyo 113-8656, Japan, E-mail: tsutsumino@thtlab.t.u-tokyo.ac.jp

[2]Asahi Glass Corporation
Hazawa-cho 1150, Kanagawa-ku, Yokohama, Kanagawa 221-8757, Japan

## Abstract

Microfabrication technology for free-standing parylene high-aspect-ratio structures (HARS) with embedded electrodes has been developed. Nano-metal ink is infused into capillaries in parylene HARS using the surface tension force. Micro electrodes in complex parylene springs have been successfully developed, and their robustness is demonstrated under large-amplitude in-plane vibration of the springs.

## Introduction

For mechanical transducers such as inertial sensors and linear actuators, sensitivity to external force should vary by orders of magnitude depending on the direction. The structure should be soft in the direction of interest, but at the same time, it should be rigid in the other two perpendicular directions to minimize the mechanical cross-talk. In order to realize such mechanical characteristics, high-aspect-ratio structures (HARS) are often employed.

The most straightforward approach for HARS is to use deep reactive-ion etching (DRIE) of a Si substrate, such as the Bosch process [1]. HEXSIL [2, 3] and HARPSS [4] have also been proposed for high-aspect-ratio structures, where deep trenches are refilled with poly-Si. However, since both single-crystal Si and poly-Si are brittle, mechanical failure is of considerable concern. Alternatively, high-aspect-ratio metal structures can be fabricated by the LIGA [5] process, but it requires X-ray, which is generally a much more expensive process. Moreover, all the conventional technologies use materials with a large Young's modulus of 100 GPa or higher.

Parylene (poly-para-xylylene) is known as a MEMS-compatible polymer that can be deposited with a CVD process, and is now attracting increasing attention for possible use in mechanical and fluidic micro devices [6-9]. Its physical properties and detailed internal stress characteristics have previously been reported [10,11]. The advantage of using parylene for mechanical parts is three-folds; Firstly, parylene has a small Young's modulus (~4GPa), which makes it easy to design soft springs with. Secondly, parylene is a non-brittle material with a large linear-elastic range (yield strain~3%), which allows a large deflection without failure. Thirdly, parylene has a 30% lower TCE than other polymers such as SU-8 and polyimide.

Recently, Suzuki & Tai [12] develop a novel microfabrication technology for high-aspect-ratio parylene structure for soft spring applications. They have developed parylene beams with widths of 10-40 μm and aspect ratios of 10-20. However, it is not straightforward process to realize electronic contact through the parylene HARS, due to relatively poor adhesion of an evaporated thin metal film on the parylene springs with narrow widths (~20 μm).

Nano-metal ink is a relatively-new electrode material, and offers possibility of flexible electrodes in MEMS structures. However, the minimum feature of conventional deposition processes such as ink-jet printing remains around 50 μm, even if the surface tension and viscosity of the ink are optimized.

The final goal of the present study is to develop a microfabrication technology to be used to produce soft springs with embedded electrodes for in-plane transducers such as accelerometers [13,14] and energy harvesting devices [15,16]. To do this, we fabricate micro electrodes in parylene HARS using nano-metal ink.

## Capillary-Force-Driven Infusion of Nano-metal Ink into Parylene HARS

In the process for parylene HARS, deep trenches etched into Si substrates are employed as the molds and refilled with parylene [12]. Figure 1 shows an SEM image of 10-30 μm-wide trenches after the deposition of 20 μm-thick paryelne-C. Clearly, a small void can be seen inside. The void is formed because the top part of the trench is sealed before the whole trench is filled with parylene. For the 20 μm-

wide trench, the width of the void is about 3 μm. When the deposition thickness of parylene-C is smaller than 10 μm, the top part of the trench is not closed, and a parylene trench is formed after the deposition.

In the present study, the capillary force is employed for the infusion of nano-metal ink (L-Ag1TeH, ULVAC) into the parylene trenches/ voids. The ink contains 60 wt% of silver in tetradecane ($C_{14}H_{30}$) solvent. The contact angle of the ink on parylene-C surface is about θ=18 deg.

The liquid column length $L$ for a surface-tension driven flow in microchannels can be written as,
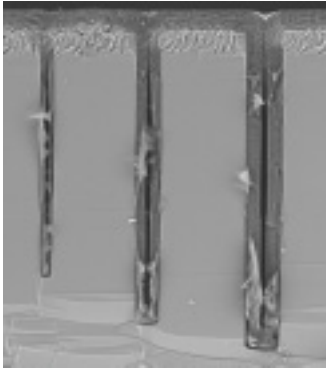


Figure 1. Cross-sectional SEM image of 10, 20, and 30 μm-wide trenches after the deposition of 20 μm- thick parylene-C.
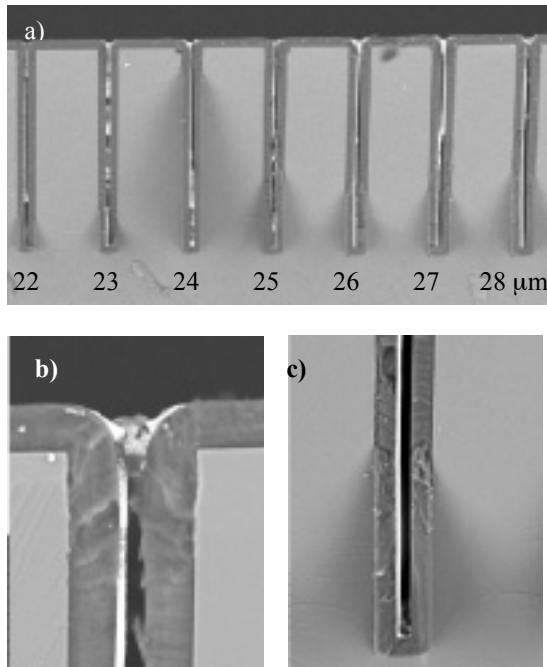


Figure 2. Cross-sectional SEM images of Si trenches with different width after infusion of nano-metal ink. Thickness of parylene-C is 12 μm. a) from left to right, 22-28 μm-wide trenches, b), c) close-up view of 28 μm-wide trench.

$$L \sim \sqrt{\frac{h\gamma_{la}\cos\theta}{3\mu}t}, \qquad (1)$$

where $h$, $\gamma_{la}$, $\theta$, $\mu$, and $t$ are respectively the channel height, surface tension, contact angle, viscosity and the elapsed time [17,18]. The surface tension and the viscosity of the nano-metal ink are respectively 25-30 mN/m and $10\,mPa\cdot s$. From Eq.(1), it is found that a 12 mm-long trench/void of 3 μm in width can be filled in a minute, showing the effectiveness of the present electrode-formation process.

Figure 2a shows cross-sectional SEM images of Si trenches with different width after infusion of the nano-metal ink. Thickness of parylene-C is 12 μm. For narrower trenches than 20 μm in width, no ink can be seen inside. This is because the ink inlet of the trench is also sealed during the parylene deposition. Whereas Ag films are highly nonuniform for 22-25 μm-wide trenches, the Ag film is almost uniform in 26-28 μm-wide trenches, and attached to one of the side walls. Therefore, the deposition thickness of parylene should be optimized to have good uniformity of the nano-metal-ink-based electrode in deep parylene trenches. Note that the top part is not sealed for Si trenches wider than 22 μm.

## FABRICATION PROCESS

Figure 3 show the main fabrication process for a free-standing parylene HARS with nano-metal-ink-based electrodes. In the present process for test
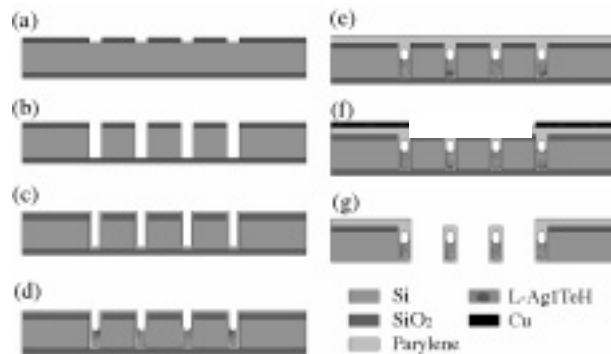


Figure 3. Fabrication process of parylene HARS with embedded electrode.
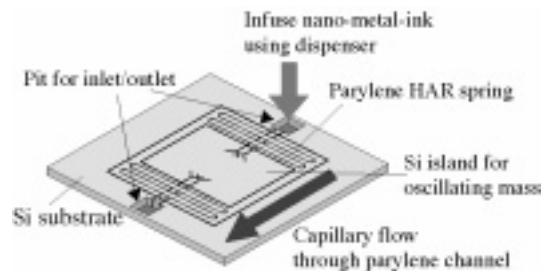


Figure 4. Schematic of nano-metal-ink infusion process.

structures, the deposition thickness of the first parylene layer was not optimized, and the electrode was sandwiched with two parylene layers.

The process start with a 3" Si wafer with 2 μm-thick thermal oxide. The upper $SiO_2$ is patterned with BOE (Fig. 3a) for the etch mask of DRIE, and 400 μm-deep trenches are etched into the substrate (Fig. 3b). The trenches are used as the parylene molds. Some of the trenches also defines the boundaries of Si islands to be left. Next, 5 μm-thick parylene-C is deposited (Fig. 3c). Then, nano-metal ink is infused through the trench using the capillary effect from a pit (1.3 x 1.3 mm$^2$) on the substrate (Fig. 4). This is followed by a bake at 150 ºC for 1 hour (Fig. 3d). Second parylene layer 15 μm in thickness is then deposited to refill the trenches (Fig. 3e). After metal mask is evaporated and patterned (Fig. 3f), the parylene film is etched with $O_2$ plasma. Finally, the Si substrate surrounding the springs is etched with $XeF_2$ to obtain free-standing structures (Fig. 3g).

## EVALUATION OF PARYLENE HARS WITH EMBEDDED ELECTRODE

Figure 5 shows a Si mass supported with a pair of high-aspect-ratio parylene springs. Dimensions of the Si mass are 2.0 mm x 2.7 mm. Beam width and height are respectively 20 and 230 μm, which corresponds to an aspect ratio of 11.5. A Y-shaped trench etched into the substrate works well as an anchor. Si islands surrounded by the parylene beams are successfully etched out with $XeF_2$, and only free-standing complex parylene structures remain. The electric resistance between the pad on the substrate and the Si island through the parylene springs is around 100 Ω. The sheet resistance of the electrode is estimated to be 4 Ω/square.

Figure 6 shows the experimental setup for the measurement of resonant frequency and electric resistance of the present device. The device was glued onto a loud speaker and shaken in the in-plane direction at prescribed frequencies and amplitudes. Relative displacement of the Si mass to the substrate was measured visually using a CCD camera equipped with a high magnification lens. Since the framing speed of the CCD camera is much slower than the oscillation frequency, the amplitude of the Si mass is measured with the streak length of the surface pattern.

Figure 7 shows the frequency response of the test structures with different beam widths. The resonant frequency $f_{res}$ is as low as 81, 155, and 270 Hz respectively for 20, 30, and 40 μm-wide beams. The peak-to-peak amplitude at the resonance is as large as 300 μm. The resonant frequencies are somewhat larger than those for parylene beams. It is found that
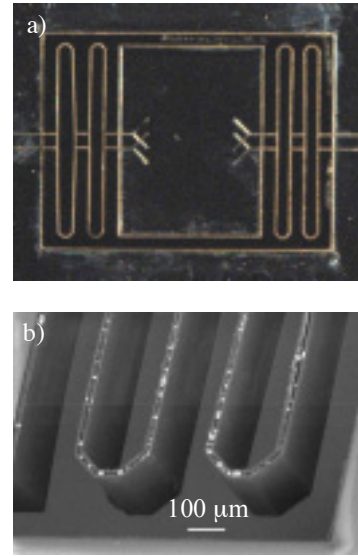


Figure 5. a) Photo of a test structure supported with a pair of parylene high-aspect-ratio springs, b) Magnified SEM image of the spring.
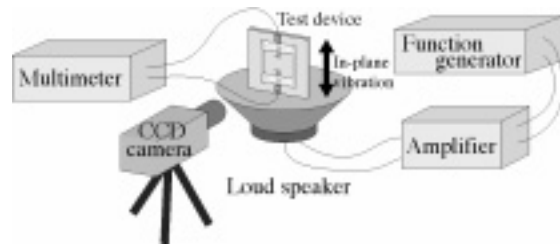


Figure 6. Experimental setup.
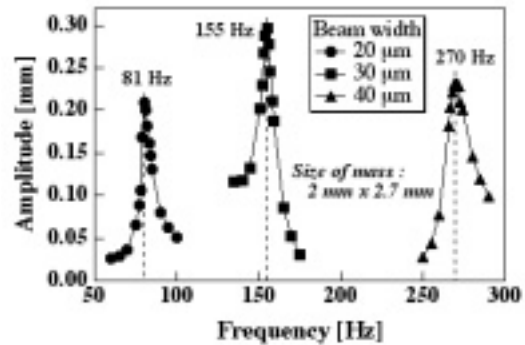


Figure 7. Frequency response of test structures with the high-aspect-ratio springs.
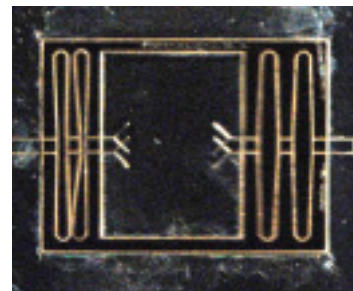


Figure 8. A snap shot of the test structure under the resonant-frequency in-plane vibration at 81 Hz.
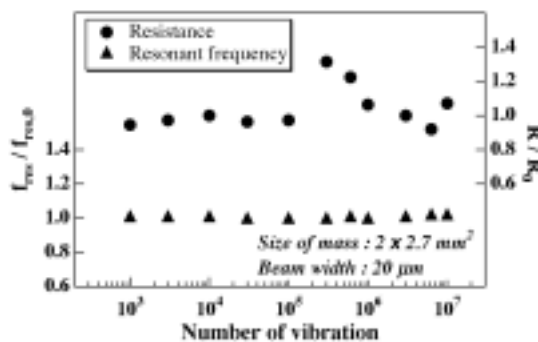
Figure 9. Long-term stability of the resonant frequency and electrical resistance.

the spring constant becomes about 50-80 % larger by the infusion of nano-metal ink. Figure 8 shows a snap-shot of the test structures at the resonant frequency of 81 Hz. Because of the large oscillation amplitude, beams on the shrunk side are almost attached to each other. However, the springs undergo neither any damage nor plastic deformation.

Figure 9 shows the resonant frequency $f_{res}$ and the resistance $R$ across the parylene beams versus cycles of the large-amplitude vibration at the resonant frequency. The resonant frequency and the resistance are nondimensionalized with their initial values. It is found that the resonant frequency of the test structure remains unchanged even after being driven at their resonant frequency oscillation for $10^7$ cycles. The electric resistance is somewhat unstable probably due to the present electric contact method to the nano-metal-ink-based electrodes, but it is also almost constant. These findings confirm the robustness of the present parylene beams with nano-metal-ink-based electrodes, which is attributed to the large yield strain of parylene and the flexibility of the metal layer made of nano-metal ink.

## CONCLUSIONS

In the present study, we propose a versatile micro electrode fabrication technology using infusion of nano-metal ink into trenches of parylene high-aspect-ratio structures for the first time. The minimum line width of the electrode can be as small as a few μm. Parylene high-aspect springs with the electrode has been successfully developed, and their robustness is demonstrated under large-deformation oscillation.

## REFERENCES

[1] A. A. Ayon, R. Braff, C. C. Lin, H. H. Sawin and M. A. Schmidt, J. Electrochem. Soc., Vol. 146, (1999), pp. 339-349.
[2] C. Keller, and M. Ferrari, Proc. Solid-state Sensor and Actuator Workshop, Hiton Head, (1994), pp. 132-137.
[3] D. A. Horsley, M. B. Cohn, A. Singh, R. Horowitz and A. P. Pisano, J. Microelectromech. Syst., Vol. 7, (1998), pp. 141-148.
[4] F. Ayazi and K. Najafi, J. Microelectromech. Syst., Vol. 9, (2000), pp. 288-294.
[5] H. Guckel, Proc. IEEE, Vol. 86, (1998), pp. 1586-1593.
[6] L. Kicklider, X.-Q. Wang, A. Desai, Y.-C. Tai, and T. D. Lee, Anal. Chem., Vol. 72, (2000), pp. 367-375.
[7] T. N. Pornsin-sirirak, Y.-C. Tai, H. Nassef, and C.-M. Ho, Sensors Actuators, A, Vol. 89, (2001), pp. 95-103.
[8] M. N. Niu, and E.-S. Kim, J. Microelectromech. Syst., Vol. 12, (2003), pp. 892-898.
[9] J. Xie, J. Shih, Q. A. Lin, B. Z. Yang, and Y.-C. Tai, Lab on Chip, Vol. 4, (2004), pp. 495-501.
[10] S. Dabral, J. Vanetten, X. Zhang, C. Apblett, G. R. Yang, P. Ficalora, and J. F. McDonald, J. Electronic Materials, Vol. 21, (1992), pp. 989-994.
[11] T. A. Harder, T.-J. Yao, Q. He, C.-Y. Shih, and Y.-C. Tai, Proc. 15th IEEE Int. Conf. MEMS, Las Vegas, (2002), pp. 17-20.
[12] Y. Suzuki, and Y.-C. Tai, J. Microelectomech. Syst. Vol. 15, (2006), pp. 1364-1370.
[13] Luo, H., Zhang, G., Carley, L. R., and Fedder, G. K., J. Microelectromech. Syst., Vol. 11, (2002), pp. 188-195.
[14] J. Chae, H. Kulah, K. Najafi, J. Microelectromech. Syst., Vol. 13, (2004), pp. 628-635.
[15] P. D. Mitcheson, T. C. Green, E. M. Yeatman, and A. S. Holmes, J. Microelectromech. Syst., Vol. 13, (2004), pp. 429-440.
[16] T. Tsutsumino, Y. Suzuki, and N. Kasagi, IEEE Int. Conf. MEMS 2006, Istanbul, (2006), pp. 98-101.
[17] Huang, W., Bhullar, R. S., and Fung, Y.-C., Trans. ASME: J. Biomech. Eng., Vol. 123, (2001), pp. 446-454.
[18] Yang, L.-J., Yao, T.-J., and Tai, Y.-C., J. Micromech. Microeng., Vol. 14, (2004), pp. 220-225.